Hierarchical ZSM-5 beads composed of zeolite nanosheets obtained by pseudomorphic transformation

Kassem Moukahhal, T.Jean Daou, Ludovic Josien, Habiba Nouali, Joumana Toufaily, Tayssir Hamieh, Anne Galarneau, Bénédicte Lebeau

Hierarchical ZSM-5 beads composed of zeolite nanosheets obtained by pseudmorphic transformation

Kassem Moukahhal,[1,2,3] T. Jean Daou,[1, 2] Ludovic Josien,[1,2] Habiba Nouali,[1,2] Joumana Toufaily,[3] Tayssir Hamieh,[3] Anne Galarneau[4] and Bénédicte Lebeau[1, 2*]

[1] Université de Haute Alsace (UHA), CNRS, IS2M UMR 7361, F-68100 Mulhouse, France

[2] Université de Strasbourg, France

[3] Laboratory of Materials, Catalysis, Environment and Analytical Methods Faculty of Sciences, Section I, Lebanese University Campus Rafic Hariri, Hadath, Lebanon

[4] Institut Charles Gerhardt Montpellier, UMR 5253 CNRS - Univ Montpellier - ENSCM, ENSCM, 240 Av. du Pr. Emile Jeanbrau, CS 60297, 34296 Montpellier Cedex 5, France

[*]*Corresponding author*

Abstract

The concept of pseudomorphic transformation was used to transform amorphous mesoporous silica beads with different size (20, 50 and 75 µm) into hierarchical MFI-type zeolite beads composed of ZSM-5 nanosheets. The beads were synthesized under hydrothermal conditions at different temperatures and treatment times, with and without mechanical stirring? (à quelle étape?). The influence of the different synthesis parameters was investigated by X-Ray Diffraction, Scanning Electron Microscopy, Transmission Electron Microscopy, X-Ray Fluorescence, Nitrogen adsorption-desorption measurements, ^{27}Al solid-state Nuclear Magnetic Resonance, Energy-Dispersive X-Ray analysis and Thermogravimetric analysis. Well-crystallized 20 µm ZSM-5 nanosheets beads similar in size and shape to the original mesoporous amorphous silica beads were obtained after a hydrothermal treatment at 150 °C for 5 days in a tumbling oven and 2 days in static at 120 °C. The influence of the bead size on the pseudomorphic transformation was studied in order to prepare well-crystallized ZSM-5 nanosheets beads of 50 and 75 µm. Results showed that the required time of the static treatment at 120°C increases when the size of the parent silica spheres increases. This is explained by the fact that crystallization starts from the outer bead surface toward the center.

Keywords: Hierarchical zeolite, ZSM-5, MFI, Nanosheets, Pseudomorphic transformation, Shaping, Beads

1 Introduction

Zeolites are microporous aluminosilicate crystalline materials that have interesting properties for wide applications in catalysis, adsorption, ion-exchange, as well as for membrane and sensor technologies [1–11]. Zeolites are very good candidates for physisorption of small molecules into their micropores. The capacity and kinetics of pollutant adsorption, which might be sensitive to diffusion phenomena, surface and porous volume, could be improved by using nanocrystals or hierarchical zeolites (micro/mesoporous or micro/macroporous) [12-14]. Several works have been carried out to introduce mesopores into zeolite [15,16] by post-synthetic demetallation of zeolite framework [17–19], hard-templating method (zeolite crystallization within confined space) [20–23], soft-templating method (mesopore generation via supramolecular self-assembly) [24–29] and the synthesis of nanosheets or nanosponges zeolitic materials using bifunctional surfactants or organosilanes [5, 30-36]. These later possesses structure directing agent functions for the formation of the zeolite framework, and an alkyl chain for inhibiting the crystalline growth of the zeolitic phase [5, 30–35].

Conventional zeolites are usually obtained as powder products consisting in micron size isolated crystals or few crystals aggregates weakly bonded. These powders are disadvantageous for many industrial applications such as those using continuous flow processes. The development of shaping methods of these materials with controllable morphologies and sizes is of great technological importance. Zeolites are commonly shaped as beads, tablets and monoliths [37-44]. The shaping of adsorbent materials into beads is interesting because it avoids a secondary molecular contamination due to the propagation of the zeolite powder in the space to be decontaminated? Pas compris. It also leads to better mechanical stability while maintaining the adsorption properties. Different methods of zeolite bead formation are referenced in the literature. However, most of the developed shaping methods required several steps: zeolite synthesis, grinding or sieving into grains of similar size, agglomeration of grains by addition of sacrificial binders (organic such as polymers or inorganic such as clays or sodium silicate) [38, 41, 44]. Recently our group has reported the one shot synthesis of zeolite beads composed with small ZK-4 crystals with hierarchical porosity involving inter-crystalline mesopores [45]. The production of ZK-4 zeolite microspheres was realized by using ion-exchange resins as shape directing macrotemplates.

An interesting one-step method for materials shaping is the pseudomorphic transformation [46]. This is the result of a slow dissolution of the starting material, which simultaneously re-precipitates or re-crystallizes into another materials without any change of the macroscopic morphology. This concept has been successfully applied to the synthesis of micron-size (5 to 800 μm) spherical particles of ordered mesoporous siliceous materials such as MCM-41 and MCM-48 [47,48] and to SOD, LTA, FAU-X-type zeolites [49,50] from amorphous spherical silica particles of the same size by adapting the dissolution rate of silica to the crystallization rate of zeolites. More recently the pseudomorphic transformation of amorphous macro-/mesoporous silica monoliths into SOD and LTA zeolites was also reported [49]. The resulting LTA monoliths, which skeleton is build of zeolite nanocrystals, showed very promising results for the cleanup of radioactive aqueous effluents in continuous flow thank to their fast ion-exchange kinetic and high ion-exchange capacity due to the absence of binder [B. Said, A. Grandjean, Y. Barre, F. Tancret, F. Fajula, A. Galarneau, Microporous Mesoporous Mater., 232 (2016) 39-52.].

Hierarchized ZSM-5 nanosheets zeolites have recently attracted much attention because of their exalted catalytic or adsorption properties compared to conventional ZSM-5 zeolites [12, 51]. They are usually synthesized as micron-size zeolitic nanosheets aggregates. In the present work, the concept of pseudomorphic transformation was used to transform amorphous silica beads with different size (20, 50 and 75 μm) into hierarchical zeolite beads composed of ZSM-5 zeolite nanosheets. Their structural and textural properties was characterized using XRD, SEM, TEM, XRF, ^{27}Al solid-state NMR, EDX, TGA and N_2 physisorption techniques.

2 Experimental section

2.1 Synthesis of the bifunctionnal structure directing agent

The di-quaternary ammonium-type surfactant used for the transformation of amorphous silica beads into MFI-type nanosheets beads, $[C_{22}H_{45}–N^+(CH_3)_2–C_6H_{12}–N^+(CH_3)_2–C_6H_{13}]Br_2$ named $C_{22\text{-}6\text{-}6}$ was obtained in two steps following the procedure reported by Choi *et al.*[5] The surfactant was composed of a long-chain alkyl group (C_{22}) and two quaternary ammonium groups spaced by a C_6 alkyl linkage.

2.2 Pseudomorphic synthesis of ZSM-5 nanosheets beads

Pseudomorphic transformation were performed by using commercial amorphous mesoporous silica beads Silica*Sphere*™ delivered by *Silicycle*®. These mesoporous silica beads have sizes of 20, 50 and 75 µm and mean pore diameters of 6 or 8 nm (data given by the supplier). Prior their use they were characterized to check their structural and textural properties (Figure S1, Table S1).

For the synthesis of ZSM-5 nanosheets beads, the protocole for ZSM-5 nanosheets reported by Choi *et al* was followed by replacing the silica source by the commercial amorphous mesoporous silica beads [5]. First, 0.40 g sodium hydroxide (Carlo Erba, 99%) and 0.11 g $Al_2(SO_4)_3.18H_2O$ (Rectaptur, 99%) were dissolved in 12 g of deionized water in a beaker. Then, 1.35 g $C_{22\text{-}6\text{-}6}$ and 0.31 g sulfuric acid (Aldrich, 96%) were added under stirring. After homogenization, the solution is transferred into a 45 mL Teflon-lined stainless steel autoclave containing 1 g of amorphous mesoporous silica beads 20, 50 or 75 µm to set the molar composition of the gel to: 1 SiO_2: 0.3 Na_2O: 0.01 Al_2O_3: 0.18 H_2SO_4: 0.1 $C_{22\text{-}6\text{-}6}$: 40 H_2O. The solution was then stirred (comment? Barreau magnétique? Vis d'Archiede?) at 250 rpm during 4 h at 60 °C prior to be placed in a tumbling oven (30 rpm) at 150 °C for 5, 7 and 10 days and placed in static (or not) in an oven at 120 °C for 1 to 5 days. (Pourquoi le traitement à 120°C est nécessaire?)

After synthesis, the product was recovered by filtration, washed with distilled water and dried overnight at 80 °C. The $C_{22\text{-}6\text{-}6}$ surfactant was removed by calcination in a furnace at 550 °C for 8 h. The resulting zeolite samples are named B-$a_{x\text{-}y}$, where "a" stands for beads size as given by the supplier, "x" stands for the number of hydrothermal treatment days at 150 °C in tumbling oven and "y" stands for the number of hydrothermal treatment days at 120 °C in static mode.

For comparison, a reference ZSM-5 nanosheet powder material was synthetized at 150 °C for 5 days under stirring (tumbling oven at 30 rpm) using tetraethoxysilane (TEOS, Aldrich, 98%) as silica source instead of amorphous mesoporous silica beads.

2.3 Characterizations

X-ray diffraction patterns of the different materials introduced in a glass capillaries were recorded using a STOE STADI-P diffractometer operating with Cu $K\alpha_1$ radiation (λ = 0.15406 nm) in the range $3< 2\theta <50$ °.

The morphology, homogeneity and particle sizes of the synthesized materials were investigated using a transmission electron microscopy (TEM) JOEL model ARM-200F, under an acceleration voltage of 200 kV, with a point-to-point resolution of 80 pm and a scanning electron microscope (SEM) (Philips, XL30 FEG) equipped with an energy dispersive X-ray analyzer (EDX) (Oxford, Inca Energy Si(Li)). In order to investigate the chemical composition of the inner part of the beads with EDX, samples were embedded in cold mounting epoxy type resin (Struers, Epofix). Embedded beads were then grinded with various SiC grinding papers and finally polished with diamond polishing suspension (particle size 1μm) till obtaining a soft surface.

Nitrogen adsorption–desorption isotherms were obtained at -196 °C using a Micromeritics ASAP 2420 apparatus. The samples were out-gassed under vacuum for 1 h at 90 °C then at 300 °C overnight before the measurements. Specific surface area was calculated according to the BET method. The total pore volumes were determined at $p/p° = 0.99$. The pore size distributions were obtained from the adsorption branch by applying DFT method that is reliable over the complete range of micro- and mesopores [52, 53]. The microporous volumes of parent silica beads and ZSM-5 nanosheets materials (beads and powder) were deduced from the cumulative volume determined by DFT method.
Thermogravimetric analyses were carried out on a METTLER TOLEDO TG/DSC STARe system with a heating rate of 5 °C/min^{-1} from 20 to 800 °C under air.

Si/Al molar ratios were calculated after determining the elemental composition of the different materials by using X-ray fluorescence spectrometry (XRF) performed on a PANalytical model Zetium.

^{27}Al ($I = 5/2$) MAS NMR spectra were recorded on a Bruker Advance II 400 MHz spectrometer operating at a frequency of 104.2 MHz at room temperature, with a Bruker

double-channel 4 mm Bruker MAS probe. Samples were spun at 12 KHz and free induction decays (FID) were collected with a $\pi/12$ pulse (0.5 µs) and a recycle delay of 1 s. Measurements were carried out with $[Al(H_2O)_6]^{3+}$ as external reference. Spectra deconvolutions were realized with DMFIT software [54].

3 Results and discussion

3.1 Amorphous mesoporous silica beads

X-ray diffraction (XRD) patterns of all the starting silica beads show a very broad peak between 20° and 30° 2θ indicating the presence of amorphous silica. The nitrogen adsorption–desorption isotherms are type I and IV (according to an IUPAC classification) [55] characteristic of microporous and mesoporous materials, respectively (Figure S1). The presence of secondary microporosity was confirmed by using DFT methods and an average micropore size of 1.48 nm was determined. The average bead diameters were determined from SEM images on an average of 50 particles. Bead sizes, mesopore diameters, specific surface areas, and pore volumes of the amorphous silica beads are reported in Table S1. Some slights differences in the bead average size or mean pore diameters are observed between our results and those given by the supplier. Beads average diameter was found similar for 20 µm beads (23±3 µm) but smaller than expected for 50 and 75 µm beads with a wide size distribution (40±6 and 62±16 µm, respectively).

3.2 Pseudomorphic transformation of amorphous mesoporous silica beads into hierarchical MFI-type zeolite beads

3.2.1 Pseudomorphic transformation of 20 µm amorphous silica beads into ZSM-5 nanosheet beads

3.2.1.1 Synthesis by hydrothermal treatment at 150 °C

First of all, the crystallinity and purity of the synthesized samples were checked by X-ray diffraction. Figure 1 show the X-ray diffraction patterns of samples obtained after 5, 7 and 10 days of hydrothermal treatment at 150 °C under tumbling stirring and of the ZSM-5 nanosheet reference powder sample. According to the XRD patterns reported in Figure 1, pure and well crystallized MFI-type zeolites were obtained for all of materials except for the sample

obtained after 5 days that also present a broad peak at 2θ = 20 - 30° indicating the presence of an amorphous phase. For B-$20_{5\text{-}0}$ and B-$20_{7\text{-}0}$ only the diffraction peaks relative to crystallographic planes (h0l) are properly indexed, indicating the growth inhibition along the b-axis, thanks to the use of $C_{22\text{-}6\text{-}6}$ bifunctional agent, thus leading the formation of nanosheets [5, 12, 30–33, 56, 57] as for the powder ZSM-5 nanosheets reference sample synthesized with TEOS. The presence of diffraction peaks relative to crystallographic planes (hkl) with k≠0 for B-$20_{10\text{-}0}$ indicate the presence of bigger MFI crystals.

SEM images displayed in Figure 2 show the conservation of the initial morphology of the beads after 5 days of hydrothermal treatment at 150 °C under tumbling stirring. After 7 days some beads are still observed but many small particles beside the beads are also present indicating a partial dissolution of the beads. After 10 days the sphere morphology is completely lost. Observations at high magnification reveal an increase of the crystal size with the increase of the duration of the hydrothermal treatment at 150 °C revealing the loss of the nanosheet morphology: this phenomenon called “Ostwald ripening” is observed in inorganic synthesis where small crystals dissolve to generate the growth of big crystals. This is consistent with XRD data.

The textural properties of the synthetized materials were studied by manometry adsorption-desorption of N_2 at 77 K. Figure 3 shows the isotherms of the different calcined materials obtained by pseudomorphic transformation in comparison with ZSM-5 nanosheets reference powder sample. Their textural properties are summarized in Table 1. All the isotherms are type I according to IUPAC [52] at low relative pressures and type II-b with hysteresis at high relative pressures. The presence of a hysteresis in the relative pressure range $0.4 < p/p° < 1$ is typical of lamellar materials, due to the stacking of the nanosheets. Inflexions in the isotherms of B-$20_{5\text{-}0}$ and B-$20_{7\text{-}0}$ at the relative pressures p/p° between 0.3 - 0.6 indicate a capillary condensation in mesopores (3.5 - 6.5 nm diameter) similarly to the ZSM-5 nanosheets reference powder sample due to the space between the nanosheets. The comparison with the isotherm of the parent 20 µm amorphous silica bead shows that the capillary condensation steps occur at a different relative pressures ($0.5 < p/p° < 0.8$ and $0.3 < p/p° < 0.6$ for parent silica and ZSM-5 pseudomorph, respectively) indicating that the mesopores are formed during the crystallization of ZSM-5 nanosheets. A secondary hysteresis is observed in ZSM-5 pseudomorphs at $0.8 < p/p° < 1$ corresponding to a secondary porosity with pores larger than 15 nm, which volume decreases with the synthesis duration at 150 °C. A similar behavior was reported for the pseudomorphic transformation of MCM-41. [Diffusion properties of hexane

in pseudomorphic MCM-41 mesoporous silicas explored by pulse field gradient NMR, Z. Adem, F. Guenneau, M-A. Springuel-Huet, A. Gedeon, J. Iapichella, T. Cacciaguerra, A. Galarneau, J. Phys. Chem. C, 2012, 116, 13749 – 13759 dx.doi.org/10.1021/jp210577t). In the fast intial step of transformation, the dissolution process of the primary nanoparticles (forming the parent silica particles) and the reprecipitation of MCM-41 in their interparticular voids leads to particles with two porosities homogeneously distributed in the whole particles: an ordered one due to the surfactant at 3.8 nm and a disordered one around 30 – 40 nm. In a slower second step, the restructuration of the initial MCM-41 type material with thick walls occurs and leads to MCM-41 type materials with thinner walls. This secondary evolution consists in the filling of the secondary porosity until the complete transformation of the particles into MCM-41, leading to the disappearance of the secondary porosity. This corresponds to an equilibrium between the porous particle and the external solution media, controlled essentialy by the pH and the silicates in solution. In the case of ZSM-5 pseudomorphs, ZSM-5 crystallizes in the voids in between the primary amorphous nanoparticles of silica due to their local dissolution leading to a secondary large porosity after 5 days at 150 °C. Some silica nanoparticles, presumably at the center of the particles are not dissolved leading to amorphous silica signature in XRD. For longer synthesis time, the ZSM-5 nanocrystals grow to fill the secondary porosity volume to get homogeneous particles in equilibrium with the external solution and some silicate species migrate outside the particles leading to some ZSM-5 crystallization at the exterior of the particles.

From DFT pore size distributions of transformed beads show micropores characteristics of MFI zeolite with sizes of 0.51 and 0.56 nm. Secondary micropores at 1.59 nm are observed. The corresponding microporous volume of these secondary micropores is constant (0.03 cm^3/g determined from the cumulative pore volume obtained by DFT treatment) with the increasing of the duration of the hydrothermal treatment at 150°C. Similar secondary micropores of 1.59 nm diameter are also observed for the reference ZSM-5 nanosheets powder in addition to the zeolitic micropores of 0.51 and 0.56 nm. These secondary micropores are an artifact and depends on the Si/Al ratio of ZSM-5. The inflexion in the nitrogen isotherm of ZSM-5 at $0.1 < p/p° < 0.2$ is due to a transition of nitrogen from a lattice fluidlike phase to a crystalline-like solid phase. This step in nitrogen adsorption becomes shaper then Si/Al increases and is barely observable for Si/Al = 20. [Adsorption by MFI-type zeolites examined by isothermal microcalorimetry and neutron diffraction. 2. Nitrogen and carbon monoxide, P.L. Llewellyn, J.-P. Coulomb, Y. Grillet, J. Patarin, G. Andre, J.

Rouquerol, Langmuir, 1993, 9, 1852 – 1856] For Si/Al around 50 as in this study, such transition can encountered for a peak in DFT calculation.

It is noteworthy that the DFT pore size of conventional MFI microcrystals (Quel Si/Al?) shows only zeolitic micropores with size of 0.51 and 0.56 nm with a related microporous volume of 0.12 cm^3/g. The crystallization rates of ZSM-5 nanosheets beads obtained by pseudomorphism were thus estimated by comparing the microporous volumes corresponding to zeolitic micropores with size of 0.51 and 0.56 nm with the one of the reference ZSM-5 nanosheets powder (0.12 cm^3/g). An increase in the zeolitic microporous volume from 0.05 cm^3/g (B-$20_{5\text{-}0}$) to 0.11 cm^3/g (B-$20_{10\text{-}0}$) is observed while increasing the hydrothermal treatment time at 150 °C from 5 to 10 days, respectively. Since the zeolitic micropore volume of the reference ZSM-5 nanosheets is 0.12 cm^3/g, it is assumed that B-$20_{10\text{-}0}$ is composed of mainly crystalline MFI-type zeolite. The crystallization rate increase from 42.3 % (B-$20_{5\text{-}0}$) to 91.7% (B-$20_{10\text{-}0}$), while increasing the duration of the hydrothermal treatment at 150 °C from 5 to 10 days, respectively. The low crystallization rate of ZSM-5 nanosheets B-$20_{5\text{-}0}$ is in agreement with the presence of an amorphous phase observed by XRD.

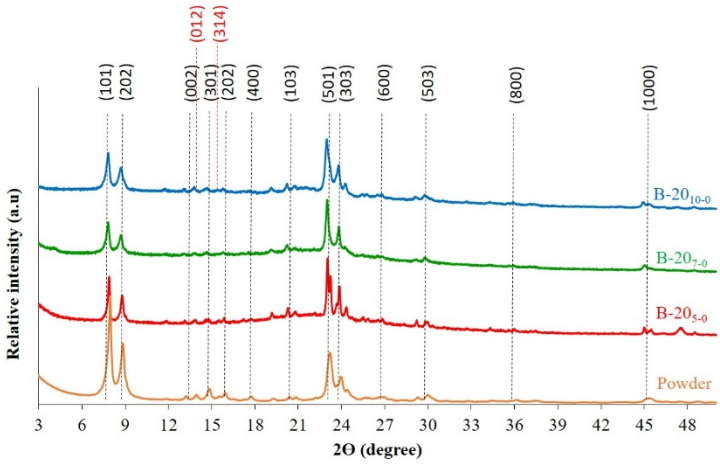

Figure 1. XRD patterns of ZSM-5 nanosheets materials obtained by pseudomorphic transformation after 5, 7 and 10 days at 150 °C with stirring and of the ZSM-5 nanosheets reference powder sample.

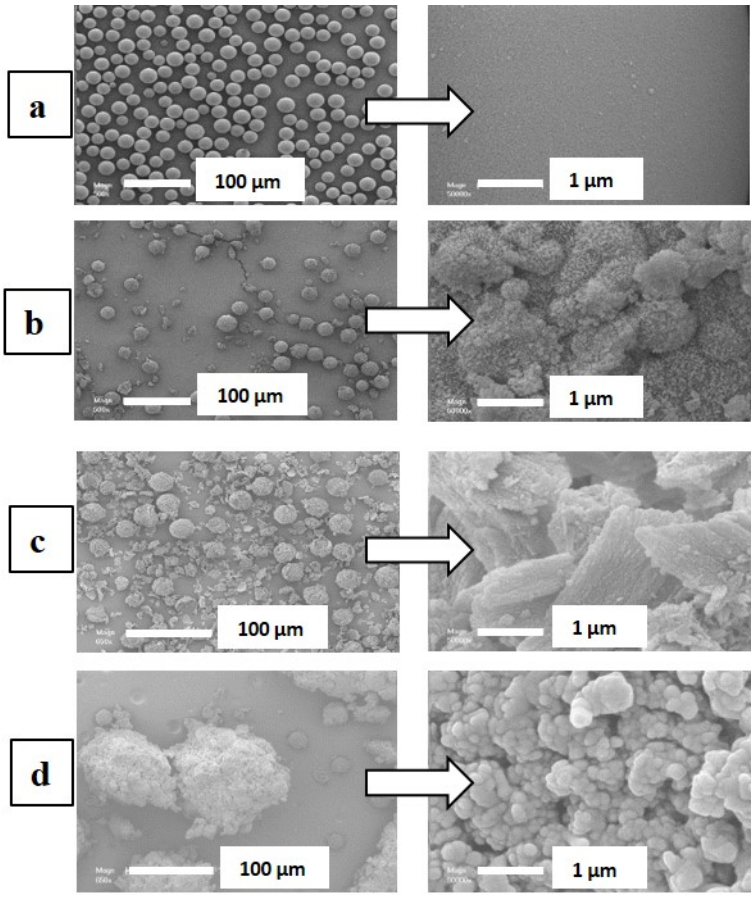

Figure 2. SEM images at low (left) and high magnification (right) of (a) the initial 20 µm amorphous silica beads and of the (b) B-$20_{5\text{-}0}$ (c) B-$20_{7\text{-}0}$ and (d) B-$20_{10\text{-}0}$ materials obtained by pseudomorphic transformation.

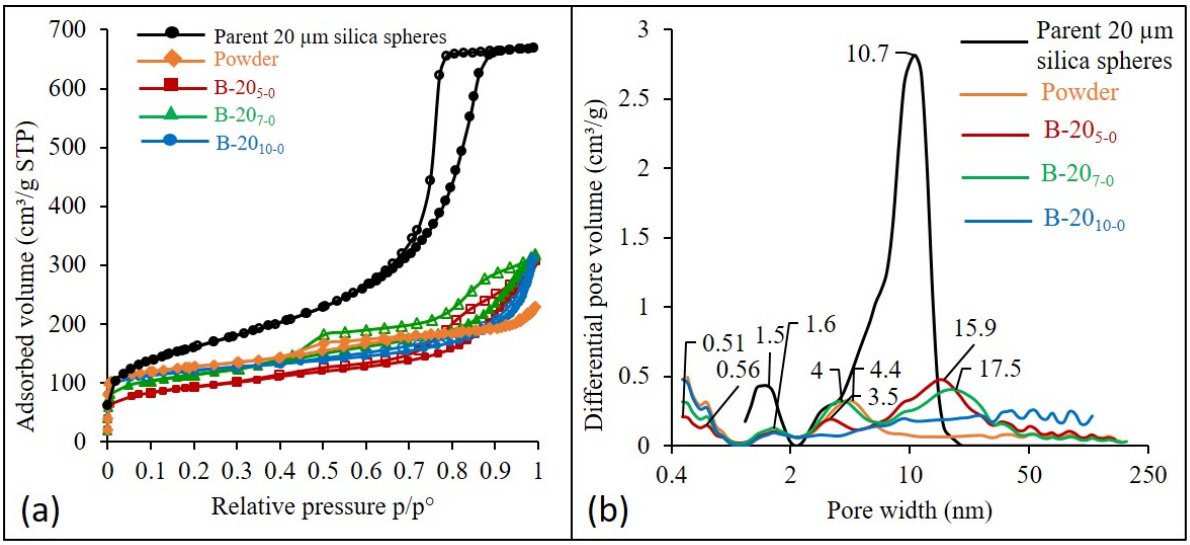

Figure 3. (a) N_2 adsorption-desorption isotherms at 77 K and (b) DFT pore size distributions determined from the adsorption branch of the N_2 isotherms of the parent 20 μm silica spheres, B-$20_{5\text{-}0}$, B-$20_{7\text{-}0}$ and B-$20_{10\text{-}0}$ calcined materials obtained at 150 °C and ZSM-5 nanosheets reference powder sample.

Table 1. Textural properties of the calcined ZSM-5 nanosheets materials synthetized by pseudomorphic transformation and of the ZSM-5 nanosheets reference powder sample

[a] *Specific surface area determined by using BET (Brunauer-Emmet-Teller) method*

[b] *Total pore volume determined at the relative pressures p/p°= 0.99. It is noteworthy that for*

	S_{BET}[a] (m^2/g)	V_{tot}[b] (cm^3/g)	V_{micro}[c] (cm^3/g)		V_{meso}[d] (cm^3/g)	Mesopores diameter[e] (nm)	Crystallization rate[f] (%)
			zeolitic	secondary			
Reference ZSM-5 nanosheets	486	0.37	0.12	0.02	0.19	4.4	100
B-20$_{5-0}$	325	0.47	0.05	0.03	0.39	3.5 – 15.3	41.7
B-20$_{7-0}$	406	0.49	0.075	0.03	0.385	4 – 17.5	62.5
B-20$_{10-0}$	445	0.48	0.11	0.03	0.34	9.2	91.7
B-20$_{5-1}$	500	0.55	0.095	0.035	0.42	4.7 – 8.9	79.2
B-20$_{5-2}$	517	0.58	0.10	0.035	0.445	4.7 – 9.1	83.3
B-20$_{5-5}$	333	0.37	0.06	0.03	0.28	3.5 – 14	50
B-50$_{5-2}$	422	0.52	0.09	0.03	0.40	4.6 – 8.9	75
B-50$_{5-3}$	489	0.48	0.09	0.04	0.35	3.6 – 6.3 – 8.7	75
B-50$_{5-4}$	493	0.54	0.09	0.04	0.41	3.9 – 8.9	75
B-75$_{5-2}$	336	0.34	0.075	0.015	0.25	4.1 – 9	62.5
B-75$_{5-4}$	574	0.62	0.11	0.03	0.48	4.3 – 9	91.7

B-20$_{5-0}$ and reference powder the presence of textural porosity (type II isotherm) does not allow determining accurately the total pore volume

[c] *Microporous volume deduced from the cumulative volume determined by DFT (Density Functional Theory) method*

[d] *Mesoporous volume : $V_{meso} = V_{tot} - V_{mircro\ total}$*

[e] *Determined from the pore size distribution obtained by DFT method applied on the adsorption branch of isotherm*

[f] *Crystallisation rate*= $V_{micro\ zeolitic}/V_{micro\ zeolitic\ of\ reference\ ZSM\text{-}5\ nanosheets}$; $V_{micro\ zeolitic\ of\ reference\ ZSM\text{-}5\ nanosheets} = 0.12\ cm^3/g$

3.2.1.2 Optimization of the pseudomorphic transformation of 20 µm amorphous silica beads into hierarchical MFI-type zeolite beads with ZSM-5 nanosheets morphology.

In order to conserve the morphology of the beads and to achieve a high crystallization rate of the ZSM-5 zeolite nanosheets constituting these beads, the temperature was decreased to 120 °C and the stirring was suppressed after the first 5 days at 150 °C under tumbling stirring. (Ca donne quoi sans agitation du tout? Le "tumbling est nécessaire pour la ZSM-5?, meme ma première agitation à 60°C devrait être faite avec la vis d'Archimède)

Indeed, since the crystallization of the ZSM-5 zeolite nanosheets was initiated (41.7% of crystallization) after 5 days at 150°C, the temperature was decreased to slow down the crystal growth and thus avoid the disruption of the sphere morphology. Stirring was also stopped to avoid any mechanical constraints in order to preserve the sphere morphology. The step at 120 °C avoids the crystallization of ZSM-5 at the exterior of the particle, as this temperature is too low, but is enough to solubilize the remaining amorphous silica and favors the homogenization and grows of the crystals inside the particle as observed in pseudomorphic synthesis of MCM-41 particles [Ziad Adem, J Phys Chem C, 2012).

The X-ray diffraction patterns of the obtained materials are presented in Figure 4 (Ajouter la reference au TEOS sur la Figure 4). XRD peaks characteristic of a pure and well-crystallized MFI-type zeolite with growth inhibition along the *b*-axis characteristic of ZSM-5 nanosheets crystals (only peaks corresponding to (h0l) plans) were observed for all materials except for B-$20_{5\text{-}5}$, which presents additional peaks off (hkl) plan because of the growth of the crystals. The SEM images displayed in Figure 5 show a conservation of the sphere morphology for all the synthesized materials. The TEM images displayed in Figure 5 show a nanosheet morphology with a thickness of 2 nm for the samples B-$20_{5\text{-}1}$ and B-$20_{5\text{-}2}$. After 5 days at 120 °C an increase in the particle size is observed to reach about 3 - 4 µm. These particles are composed of the stacking of thicker zeolite sheets (see Figure 5d). Figure 6 shows the N_2 adsorption-desorption isotherms at 77 K of the calcined obtained samples. Type I isotherms at low relative pressures and type II-b isotherms at high relative pressures were observed for all samples. All the isotherms have a H3 (or H4) type hysteresis between $0.4 < p/p^0 < 1$, which is

characteristic of the lamellar materials due to the stacking of the nanosheets. A mixture of type II-b and type IV is observed for the materials B-$20_{5\text{-}0}$ and B-$20_{5\text{-}5}$. For B-$20_{5\text{-}0}$, this is the result of uncomplete pseudomorphic transformation of the particle as explained above. The longer synthesis time at 120 °C allows to homogenize the particle by dissolution of the remaining amorphous silica and the growth of the crystals inside the particles, which lead to the disappearance of the secondary pore volume. For long time duration (5 days) at 120 °C the crystals grow on the surface of the particles and give rise to a secondary pore volumes. This is accompanied by a decrease in micropore volume (for B-$20_{5\text{-}5}$, V_μ = 0.060 cm^3/g). This phenomenon can be due to a dissolution process of the nanosheets to give birth to bigger particles composed of thicker zeolite sheets whose crystallization process is not complete after 5 days at 120 °C. The textural properties of the obtained materials are reported in Table 1. The zeolitic microporous volume increased after 1 and 2 days of additional hydrothermal treatment at 120 °C (V_μ = 0.095 and 0.100 cm^3/g, respectively) compared to the material obtained only after 5 days of synthesis at 150 °C (0.050 cm^3/g). The optimal synthesis conditions seem to be 5 days at 150 °C and 2 days at 120 °C (Peut-être que 3 ou 4 jours à 120°C auraient été l'optimum?). Indeed, a zeolitic microporous volume of 0.10 cm^3/g was measured for B-$20_{5\text{-}2}$, which indicates a good crystallization rate of 83.3%. The "secondary" microporosity (due to nitrogen reorganization in the micropores) is similar for both B-$20_{5\text{-}1}$ and B-$20_{5\text{-}2}$ samples (V = 0.035 cm^3/g). The mesopores with diameters centered at around 4.7 nm are clearly observable for samples synthesized with an additional heat treatment of 1 and 2 days at 120 °C and is a sign of the structure modification of the amorphous silica beads towards well-crystallized ZSM-5 nanosheets beads. Indeed, the reference ZSM-5 nanosheets sample (powder) presents mesopores with an average diameter of 4.4 nm.

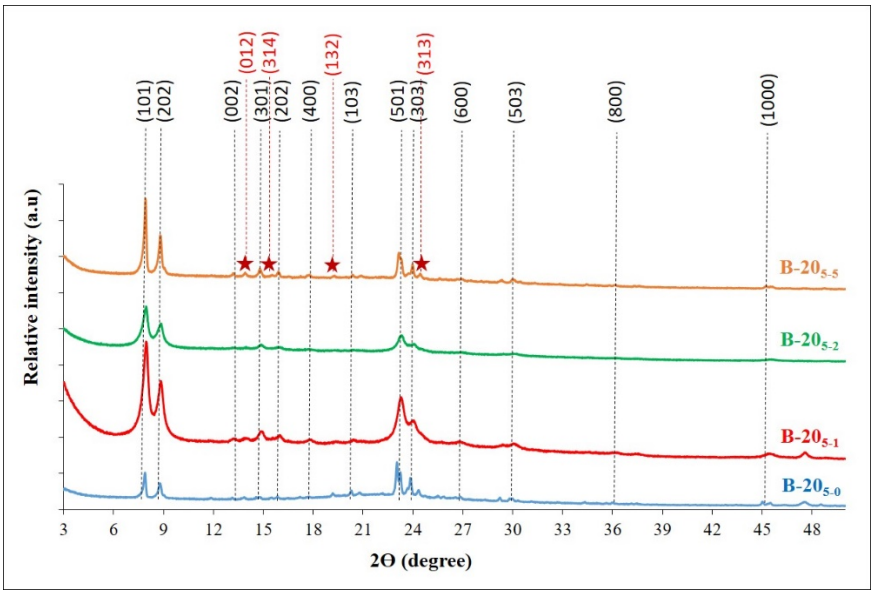

Figure 4. XRD patterns of ZSM-5 nanosheets materials obtained by pseudomorphic transformation after 5 days at 150 °C with tumbling stirring and an additional treatment for 1, 2 and 5 days at 120 °C under static conditions.

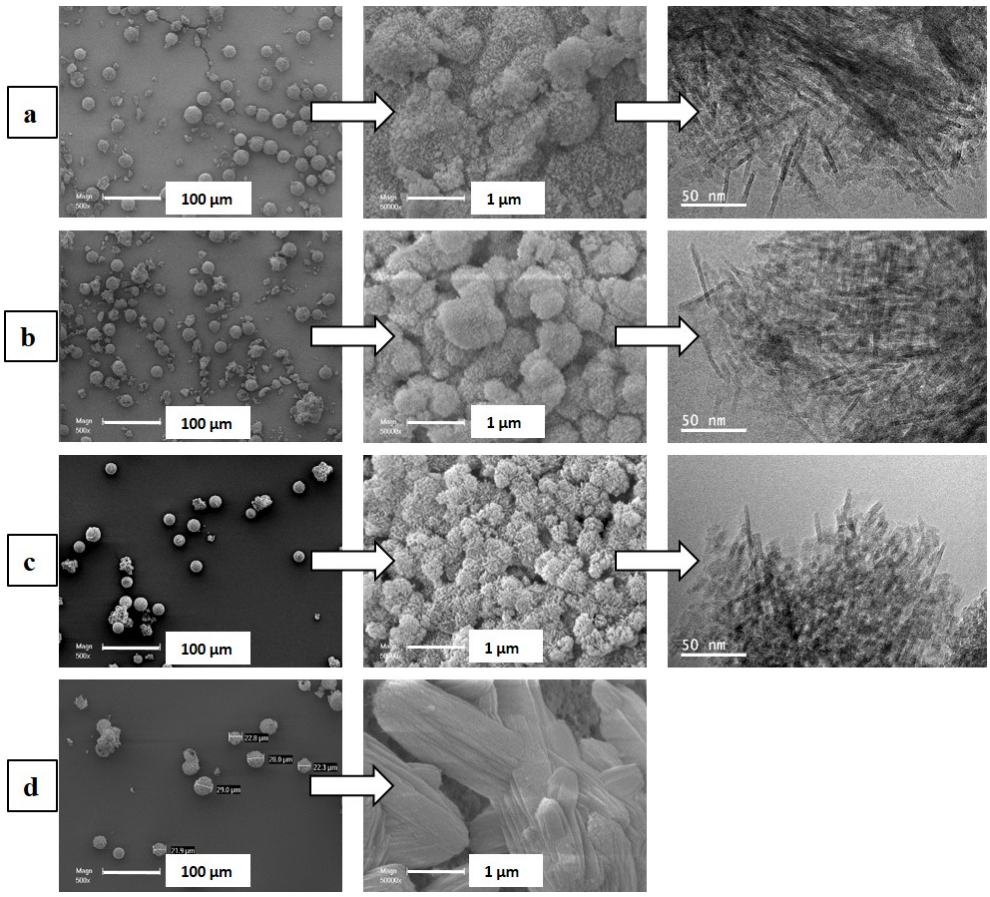

Figure 5**.** SEM and TEM images of the obtained materials for (a) 5 days at 150 °C, and with additional (b) 1, (c) 2, and (d) 5 days at 120 °C in static mode.

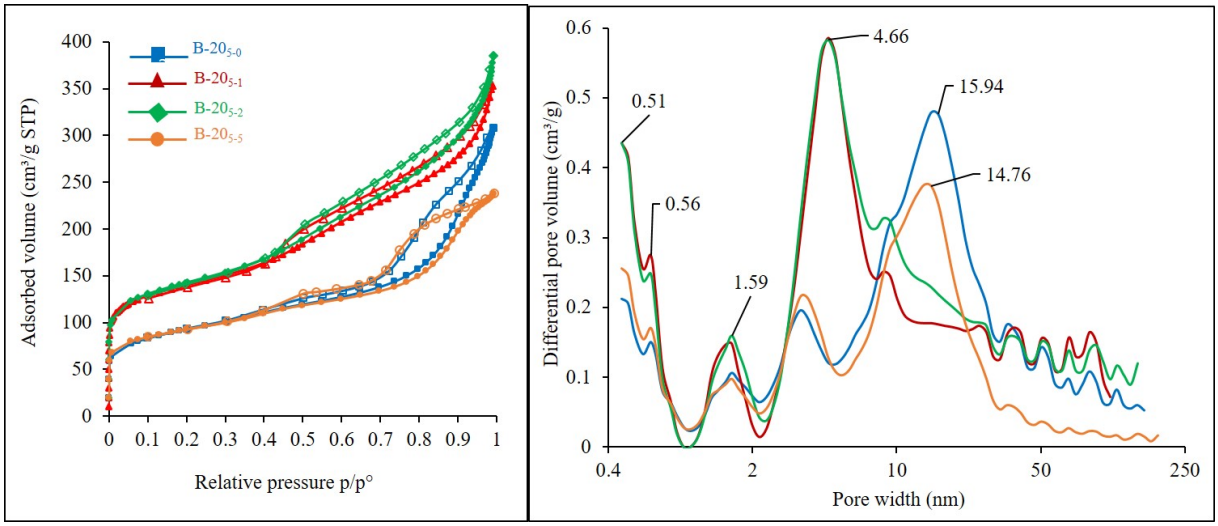

Figure 6. (a) N_2 adsorption-desorption isotherms at 77 K and b) DFT pore size distributions of the calcined materials obtained at 150 °C with an additional hydrothermal treatment for 1, 2 and 5 days at 120 °C in static mode.

3.2.2 Impact of the size of the amorphous silica beads in their pseudomorphic transformation into MFI-type zeolite beads composed of ZSM-5 nanosheets.

The pseudomorphic transformation of the amorphous silica beads into zeolites ZSM-5 depends on the kinetics of silica dissolution and ZSM-5 recrystallization. The crystallization process seems to process from the outside to the inside of the beads. In order to study the impact of the size of the amorphous silica spheres on their pseudomorphic transformation into beads composed of ZSM-5 nanosheets, syntheses were carried out on amorphous mesoporous silica beads of sizes of 50 and 75 µm. The duration of the hydrothermal treatment at 120 °C was extended starting under conditions already optimized for the 20 µm spheres (B-20$_{5-2}$ material).

Figure 7 displays the X-ray diffraction patterns of the obtained materials. XRD peaks characteristic of a pure MFI-type zeolite phase with inhibition of growth along the b-axis were observed for all synthesized materials with the 50 and 75 µm spheres. A slight hallow between 20º and 26º 2Θ characteristic of amorphous aluminosilicate material is observed for the materials obtained after 2 days of hydrothermal treatment at 120 °C from both the 50 and 75 µm beads. This indicates a decrease in the crystallization rate inside the particles with the increase of the size of the silica beads under the same synthesis conditions. This hallow is no

more observed after 3 and 4 days of hydrothermal treatment at 120 °C for 50 and 75 μm beads, respectively.

The adsorption-desorption isotherms of N_2 are presented in Figure 8a. The textural properties of the obtained materials reported in Table 1 show an increase of the BET surface with increasing the duration of hydrothermal treatment at 120 °C. Micropores characteristic of the MFI zeolite are observed for all samples (Fig. 8b). The zeolitic microporous volume of 0.09 cm^3/g corresponding to a crystallization rate of 75 % is observed after 2 days and increases for 3 and 4 days of hydrothermal treatment at 120 °C for the 50 μm spheres. Pas possible que ce soit le meme volume microporeux, l'isotherme est plus basse pour 2 jours que pour 3 et 4 jours??? ~~The "secondary" microporous volume slightly increases with the duration of the hydrothermal treatment at 120 °C from 0.03 to 0.04 cm^3/g,~~. Simultaneously, the mesopores of 3.9 - 4.6 nm are more visible after 3 and 4 days in comparison to the heat treatment for 2 days, indicating a better structuration of the ZSM-5 nanosheets. The "secondary" microporous volume slightly increases with the duration of the hydrothermal treatment at 120 °C from 0.03 to 0.04 cm^3/g, suggesting the elimination of some Al from the crystalline ZSM-5 strucuture. When amorphous mesoporous silica beads of 75 μm size are used as precursors, the transformed beads present also zeolitic micropores at 0.51 and 0.56 nm. The corresponding microporous volumes increased from 0.075 to 0.11 cm^3/g when the duration of the hydrothermal treatment at 120 °C increased from 2 to 4 days, respectively. The value of the zeolitic microporous volume (0.11 cm^3/g), after 4 days of hydrothermal treatment at 120 °C for the 75 μm spheres, corresponds to a crystallization rate of 92 %. The volume of "secondary micropores" also increased from 0.015 to 0.030 cm^3/g after 2 (B-$75_{5\text{-}2}$) and 4 (B-$75_{5\text{-}4}$) days, respectively, indicating a slightly lower incorporation of Al in the crystalline structure after 4 days. The mesopores of 4.1 - 4.3 nm diameter are clearly identified for an additional heat treatment of 4 days.

SEM images presented in Figure 9 show a conservation of the sphere morphology for all the obtained samples. Few small fragments are also observed. TEM images show a nanosheet morphology with 2 nm of size for all samples with a moderate growth of the nanosheets with the increase of the duration of the hydrothermal treatment at 120 °C.

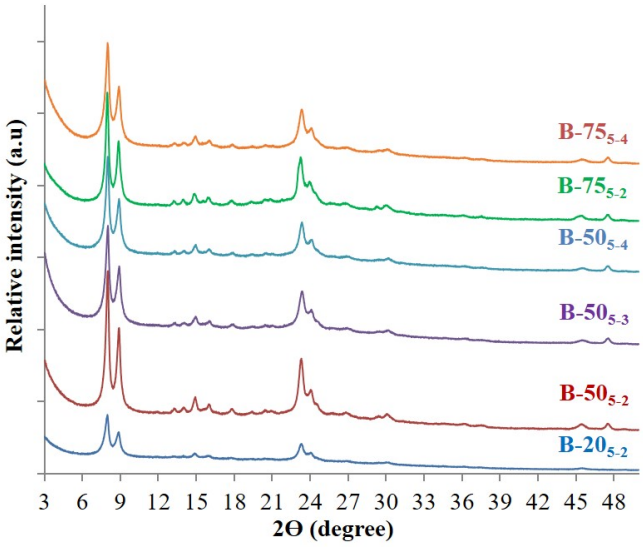

Figure 7. XRD patterns of ZSM-5 nanosheets materials obtained by pseudomorphic transformation of the 20, 50, 75 µm amorphous silica spheres.

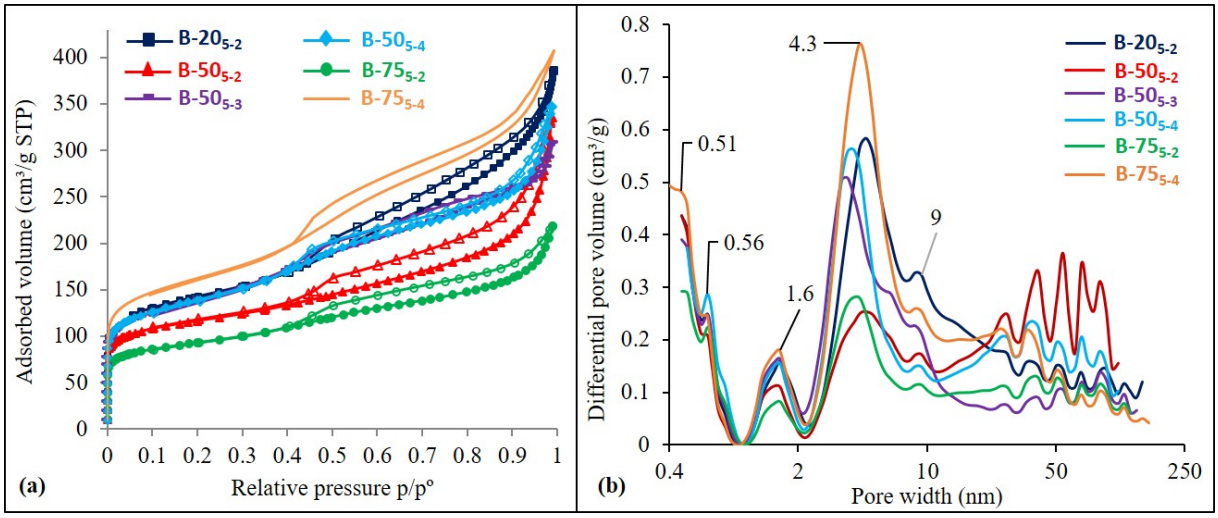

Figure 8. (a) Adsorption-desorption isotherms of nitrogen at 77 K and (b) DFT pore size distributions determined from the adsorption branch of the ZSM-5 nanosheets synthetized by pseudomorphic transformation of 20, 50 and 75 µm amorphous mesoporous silica beads.

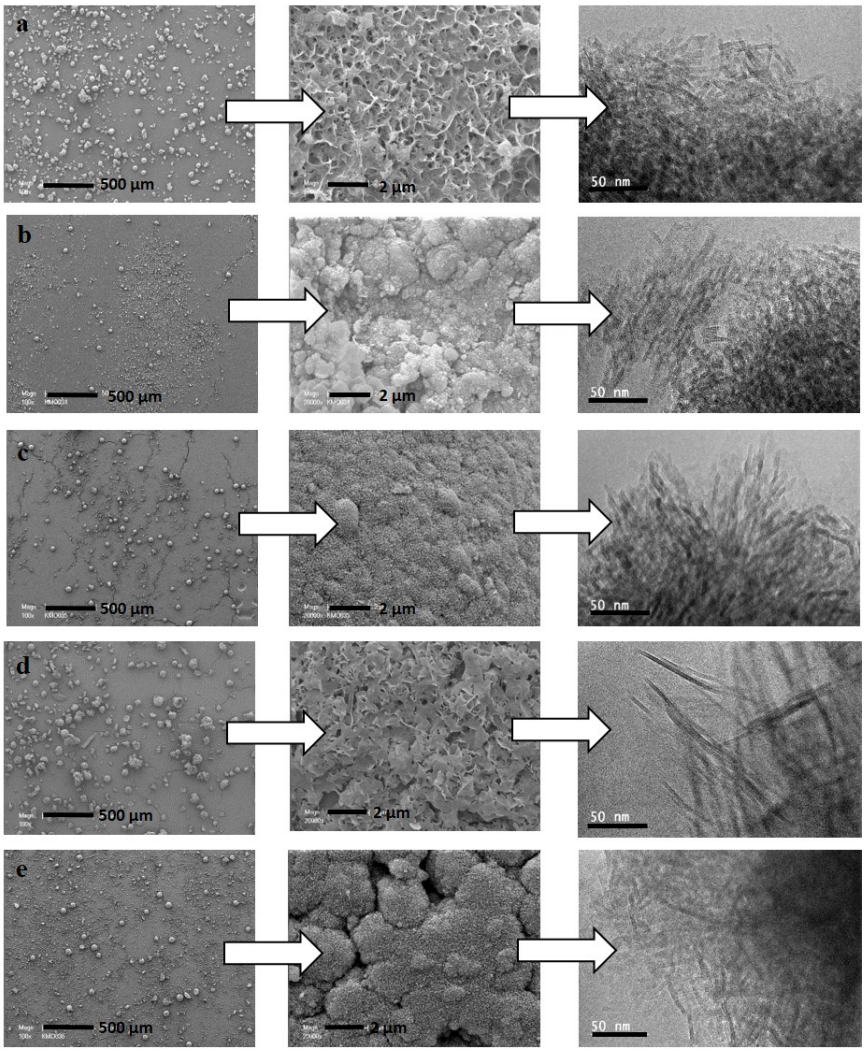

Figure 9. SEM and TEM images of the ZSM-5 nanosheet materials synthesized by pseudmorphic transformation of 50 µm amorphous mesoporous silica beads after (a) 2, (b) 3 and (c) 4 days at 120 °C and 75 µm amorphous mesoporous silica beads after (d) 2 and (e) 4 days at 120°C.

It is interesting to compare the crystallization levels (83, 75 and 62%) of the 3 materials (B-$20_{5\text{-}2}$,B-$50_{5\text{-}2}$, B-$75_{5\text{-}2}$) obtained after the same duration of hydrothermal treatments (5 days at 150°C under tumbling stirring and 2 days in static at 120°C) of the 3 parent amorphous mesoporous silica beads (20, 50 and 75 µm, respectively) to highlight the impact of the parent bead size. The pseudomorphic transformation of mesoporous amorphous silica beads into ZSM-5 nanosheets beads is slowed down with the increasing parent bead size. This is consistent with the fact that crystallization starts from the outer surface to the center of the beads.

3.2.3. Complementary characterization of ZSM-5 nanosheet beads

The ZSM-5 nanosheet materials obtained with spherical morphology were further analyzed by TGA under air. Two weight losses were observed from 20 and 800 °C (Table 2). The first one in the temperature range 30 - 110 °C corresponds to the physisorbed water and the second one in the temperature range 110 - 700 °C corresponds to the oxidation of the organic matter (bi-functionnal structuring agent). Since each unit cell of ZSM-5 contains 2 organic cations, a weight loss of 16.5 wt% is expected [12, 32, 53]. However, for all analyzed materials the weight loss corresponding to the oxidation of the organic cations is higher indicating an excess of bi-functional structure directing agent and/or some dehydroxylation of remaining amorphous silicate phases. The excess of surfactant could be decreased to 18 wt% by extraction under reflux with HCl 0.2 M/ethanol solution. The non-extractable content corresponds almost to the 2 expected bi-functionnal structuring agent per unit cell of ZSM-5 nanosheets. The extractable portion is attributed to the bi-functionnal structuring agent that form micelle on the surface of nanosheets with long alkane chains as 'dummy' filler [57]. The molar Si/Al ratio determined by XRF for all samples are reported in Table 2. This ratio was corrected from ^{27}Al MAS NMR results by considering only the molar proportion of tetrahedral coordinated aluminum inserted in the zeolitic framework. Indeed, the ^{27}Al MAS NMR spectra of samples (Figure S2), show that the aluminum is mainly present in tetrahedral coordination with a main resonance at about 50 ppm. The presence of a weak resonance was also observed at about 0 ppm indicating the presence of extra framework Al species with octahedral coordination. It is noteworthy that an average Si/Al ratio of 44 was determined for the ZSM-5 nanosheets materials obtained by pseudomorphism and it corresponds to the expected value for ZSM-5 nanosheets [12, 53].

Table 2. Thermal analysis results and Si/Al ratio of the synthetized materials.

	Physisorbed water (%)[a]	**Organic matter (%)[b]**	**Experimental number of organic cations[c] / unit cell**	**Si/Al Ratio[d]**	**Corrected Si/Al Ratio[e]**
B-20$_{5\text{-}0}$	1.3	21.6	2.6	31	33
B-20$_{5\text{-}1}$	0.5	41.3	5	35	39
B-20$_{5\text{-}2}$	0.7	43.6	5.2	41	44

B-20$_{5\text{-}5}$	1.1	20.9	2.5	59	63
B-50$_{5\text{-}2}$	3.2	34.0	4.1	33	34
B-50$_{5\text{-}3}$	1	27.4	3.3	41	44
B-50$_{5\text{-}4}$	0.9	30.9	3.7	41	50
B-75$_{5\text{-}2}$	3.9	33.8	4.1	49	49
B-75$_{5\text{-}4}$	0.8	34.9	4.2	41	44

[a] *corresponding to the mass loss determined by TGA in the temperature range 30-110 °C*

[b] *corresponding to the mass loss determined by TGA in the temperature range 110-700 °C*

[c] *structure directing agent*

[d] *determined by XRF*

[e] *values determined by XRF corrected from ^{27}Al NMR data*

ZSM-5 nanosheets materials obtained by pseudomorphism were analyzed by EDX and in all cases elemental mapping showed that Si and Al are homogeneously distributed in the beads (Figure 10) confirming once more that the beads are entirely crystallized with constant Si/Al ratio from the outside to the center of the beads.

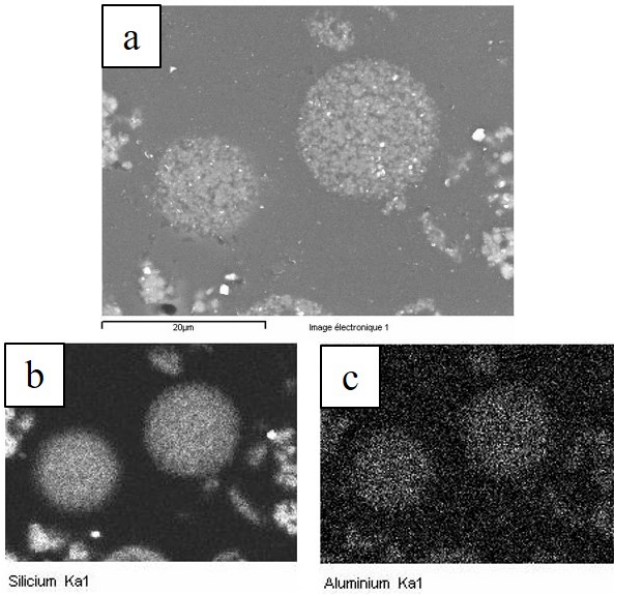

Figure 10. SEM image (a) and EDX Si (b) and Al (c) elemental mapping for B-20$_{5\text{-}2}$.

4 Conclusion

Pseudomorphic transformation of mesoporous silica beads into ZSM-5 nanosheets beads have been successfully realized from starting beads with 20, 50 and 75 µm diameter size. The formation of ZSM-5 nanosheets was confirmed by XRD with the presence of peaks characteristic of MFI zeolite with inhibition growth along b-axis and by N_2 physisorption with the presence of micropores characteristic of MFI zeolite at 0.51 and 0.56 nm and mesopores with an average diameter of 3.9 - 4.7 nm. A first hydrothermal treatment at 150°C for 5 days under tumbling stirring was found optimal to preserve the spherical morphology but not sufficient for full crystallization. A subsequent hydrothermal treatment at 120°C under static conditions was successfully applied to reach a high crystallization rate without disrupting the spherical morphology. An increase of the duration of the secondary hydrothermal treatment at 120 °C from 2 to 4 days was necessary when the bead diameter was increased from 20 to 50 or 75 µm. This result was related to the fact that crystallization starts from the outside to the inside of the beads. Almost fully crystallized ZSM-5 nanosheets beads of 20 to 75 µm were characterized with a zeolitic micropore volume of 0.11 cm^3/g and a mesopore size distribution centered at 3.9 - 4.7 nm, corresponding to the characteristics of conventional ZSM-5 nanosheets with a zeolitic micropore volume of 0.12 cm^3/g.

Acknowledgments: The XRD, NMR, adsorption, AMTR and ME platforms of IS2M are acknowledged. Laure Michelin, Severinne Rigolet and Loïc Vidal are warmly thanked for their help in XRD, NMR and TEM acquisition data, respectively.

References

[1] A. Mosca, J. Hedlund, F.N. Ridha, P. Webley, Optimization of synthesis procedures for structured PSA adsorbents, Adsorption. 14 (2008) 687–693. doi:10.1007/s10450-008-9126-9.

[2] A. Corma, State of the art and future challenges of zeolites as catalysts, J. Catal. 216 (2003) 298–312. doi:10.1016/S0021-9517(02)00132-X.

[3] M. Choi, H.S. Cho, R. Srivastava, C. Venkatesan, D.-H. Choi, R. Ryoo, Amphiphilic organosilane-directed synthesis of crystalline zeolite with tunable mesoporosity, Nat. Mater. 5 (2006) 718–723. doi:10.1038/nmat1705.

[4] R. Srivastava, M. Choi, R. Ryoo, Mesoporous materials with zeolite framework: remarkable effect of the hierarchical structure for retardation of catalyst deactivation, Chem. Commun. 0 (2006) 4489–4491. doi:10.1039/B612116K.

[5] M. Choi, K. Na, J. Kim, Y. Sakamoto, O. Terasaki, R. Ryoo, Stable single-unit-cell nanosheets of zeolite MFI as active and long-lived catalysts, Nature. 461 (2009) 246–249. doi:10.1038/nature08288.

[6] J. Kim, M. Choi, R. Ryoo, Effect of mesoporosity against the deactivation of MFI zeolite catalyst during the methanol-to-hydrocarbon conversion process, J. Catal. 269 (2010) 219–228. doi:10.1016/j.jcat.2009.11.009.

[7] J. Kim, W. Park, R. Ryoo, Surfactant-Directed Zeolite Nanosheets: A High-Performance Catalyst for Gas-Phase Beckmann Rearrangement, ACS Catal. 1 (2011) 337–341. doi:10.1021/cs100160g.

[8] I. Kabalan, I. Khay, H. Nouali, A. Ryzhikov, B. Lebeau, S. Albrecht, S. Rigolet, M.-B. Fadlallah, J. Toufaily, T. Hamieh, J. Patarin, T.J. Daou, Influence of the Particle Sizes on the Energetic Performances of MFI-Type Zeolites, J. Phys. Chem. C. 119 (2015) 18074–18083. doi:10.1021/acs.jpcc.5b04484.

[9] J. Huve, A. Ryzhikov, H. Nouali, V. Lallia, G. Augé, T.J. Daou, Porous sorbents for the capture of iodine radioactive compounds: A review, *RSC Advances*, 8 (2018) 29248-29273. doi: 10.1039/C8RA04775H.

[10] A. Said, L. Limousy, H. Nouali, L. Michelin, J. Halwani, J. Toufaily, T. Hamieh, P.Dutournié, T.J. Daou, Synthesis of mono and bi-layer MFI zeolite films on macroporous alumina tubular supports: application to nanofiltration, *Journal of Crystal Growth*, 428 (2015) 71-79. doi: 10.1016/j.jcrysgro.2015.07.028.

[11] A. Astafan, M.A. Benghalem, Y. Pouilloux, J. Patarin, N. Bats, C. Bouchy, T.J. Daou, L. Pinard, Particular properties of the coke formed on nano-sponge *BEA zeolite during ethanol-to-hydrocarbons transformation, *J. Catal.* 336 (2016) 1-10. doi: 10.1016/j.jcat.2016.01.002.

[12] I. Kabalan, B. Lebeau, H. Nouali, J. Toufaily, T. Hamieh, B. Koubaissy, J.-P. Bellat, T.J. Daou, New Generation of Zeolite Materials for Environmental Applications, J. Phys. Chem. C. 120 (2016) 2688–2697. doi:10.1021/acs.jpcc.5b10052.

[13] L. El Hanache, B. Lebeau, H. Nouali, J. Toufaily, T. Hamieh, T.J. Daou, Performance of surfactant-modified *BEA-type zeolite nanosponges for the removal of nitrate in contaminated water: Effect of the external surface, J. Hazard. Mater. 364 (2019) 206–217. doi:10.1016/j.jhazmat.2018.10.015.

[14] I. Kabalan, B. Lebeau, M.-B. Fadlallah, J. Toufaily, T. Hamieh, J.P. Bellat, T.J. Daou, Hierarchical FAU-type zeolite for molecular decontamination, *Journal of Nanoscience and Nanotechnology*, 16 (2016) 9318-9322. doi: 10.1166/jnn.2016.12884.

[15] Z.L. Hua, J. Zhou, J.L. Shi, Recent advances in hierarchically structured zeolites: synthesis and material performances, Chem. Commun. 47 (2011) 10536-10547. doi:10.1039/c1cc10261c.

[16] K. Na, M. Choi, R. Ryoo, Recent advances in the synthesis of hierarchically nanoporous zeolites, Microporous Mesoporous Mater. 166 (2013) 3–19. doi:10.1016/j.micromeso.2012.03.054.

[17] A.H. Janssen, A.J. Koster, K.P. de Jong, Three-Dimensional Transmission Electron Microscopic Observations of Mesopores in Dealuminated Zeolite Y Supported by NWO under grant 98037. The research of A.J.K. has been made possible by a fellowship of the Royal Netherlands Academy of Arts and Sciences (KNAW). The authors thank J. E. M. J. Raaymakers for the nitrogen physisorption measurements, A. J. M. Mens for the XPS measurements, J. A. R. van Veen and E. J. Creyghton for physical data and useful discussions, and Shell International Chemicals and Zeolyst for the samples., Angew. Chem. Int. Ed Engl. 40 (2001) 1102–1104.

[18] N.S. Nesterenko, F. Thibault-Starzyk, V. Montouillout, V.V. Yuschenko, C. Fernandez, J.-P. Gilson, F. Fajula, I.I. Ivanova, Accessibility of the acid sites in dealuminated small-port mordenites studied by FTIR of co-adsorbed alkylpyridines and CO, Microporous Mesoporous Mater. 71 (2004) 157–166. doi:10.1016/j.micromeso.2004.03.028.

[19] J.C. Groen, T. Bach, U. Ziese, A.M. Paulaime-van Donk, K.P. de Jong, J.A. Moulijn, J. Pérez-Ramírez, Creation of Hollow Zeolite Architectures by Controlled Desilication of Al-Zoned ZSM-5 Crystals, J. Am. Chem. Soc. 127 (2005) 10792–10793. doi:10.1021/ja052592x.

[20] E. Bekyarova, K. Kaneko, Structure and Physical Properties of Tailor-Made Ce,Zr-Doped Carbon Aerogels, Adv. Mater. 12 (2000) 1625–1628. doi:10.1002/1521-4095(200011)12:21<1625::AID-ADMA1625>3.0.CO;2-9.

[21] R. Ryoo, S.H. Joo, M. Kruk, M. Jaroniec, Ordered Mesoporous Carbons, Adv. Mater. 13 (2001) 677–681. doi:10.1002/1521-4095(200105)13:9<677::AID-DMA677>3.0.CO;2-C.

[22] Y. Fang, H. Hu, An Ordered Mesoporous Aluminosilicate with Completely Crystalline Zeolite Wall Structure, J. Am. Chem. Soc. 128 (2006) 10636–10637. doi:10.1021/ja061182l.

[23] W. Fan, M.A. Snyder, S. Kumar, P.-S. Lee, W.C. Yoo, A.V. McCormick, R. Lee Penn, A. Stein, M. Tsapatsis, Hierarchical nanofabrication of microporous crystals with ordered mesoporosity, Nat. Mater. 7 (2008) 984–991. doi:10.1038/nmat2302.

[24] U. Ciesla, F. Schüth, Ordered mesoporous materials, Microporous Mesoporous Mater. 27 (1999) 131–149. doi:10.1016/S1387-1811(98)00249-2.

[25] A. Monnier, F. Schüth, Q. Huo, D. Kumar, D. Margolese, R.S. Maxwell, G.D. Stucky, M. Krishnamurty, P. Petroff, A. Firouzi, M. Janicke, B.F. Chmelka, Cooperative Formation of Inorganic-Organic Interfaces in the Synthesis of Silicate Mesostructures, Science. 261 (1993) 1299–1303. doi:10.1126/science.261.5126.1299.

[26] M. Hartmann, Ordered Mesoporous Materials for Bioadsorption and Biocatalysis, Chem. Mater. 17 (2005) 4577–4593. doi:10.1021/cm0485658.

[27] Y. Xia, R. Mokaya, On the synthesis and characterization of ZSM-5/MCM-48 aluminosilicate composite materials, J. Mater. Chem. 14 (2004) 863–870. doi:10.1039/B313389C.

[28] P. Prokešová, S. Mintova, J. Čejka, T. Bein, Preparation of nanosized micro/mesoporous composites via simultaneous synthesis of Beta/MCM-48 phases, Microporous Mesoporous Mater. 64 (2003) 165–174. doi:10.1016/S1387-1811(03)00464-5.

[29] A. Galarneau, H. Cambon, F.D. Renzo, R. Ryoo, M. Choi, F. Fajula, Microporosity and connections between pores in SBA-15 mesostructured silicas as a function of the temperature of synthesis, New J. Chem. 27 (2003) 73–79. doi:10.1039/B207378C.

[30] K. Na, M. Choi, W. Park, Y. Sakamoto, O. Terasaki, R. Ryoo, Pillared MFI zeolite nanosheets of a single-unit-cell thickness, J. Am. Chem. Soc. 132 (2010) 4169–4177. doi:10.1021/ja908382n.

[31] K. Na, C. Jo, J. Kim, K. Cho, J. Jung, Y. Seo, R.J. Messinger, B.F. Chmelka, R. Ryoo, Directing zeolite structures into hierarchically nanoporous architectures, Science. 333 (2011) 328–332. doi:10.1126/science.1204452.

[32] J. Dhainaut, T.J. Daou, Y. Bidal, N. Bats, B. Harbuzaru, G. Lapisardi, H. Chaumeil, A. Defoin, L. Rouleau, J. Patarin, One-pot structural conversion of magadiite into MFI zeolite nanosheets using mononitrogen surfactants as structure and shape-directing agents, CrystEngComm. 15 (2013) 3009. doi:10.1039/c3ce40118a.

[33] K. Na, W. Park, Y. Seo, R. Ryoo, Disordered Assembly of MFI Zeolite Nanosheets with a Large Volume of Intersheet Mesopores, Chem. Mater. 23 (2011) 1273–1279. doi:10.1021/cm103245m.

[34] J. Jung, C. Jo, K. Cho, R. Ryoo, Zeolite nanosheet of a single-pore thickness generated by a zeolite-structure-directing surfactant, J. Mater. Chem. 22 (2012) 4637–4640. doi:10.1039/C2JM16539B.

[35] A.G. Machoke, I.Y. Knoke, S. Lopez-Orozco, M. Schmiele, T. Selvam, V.R.R. Marthala, E. Spiecker, T. Unruh, M. Hartmann, W. Schwieger, Synthesis of multilamellar MFI-type zeolites under static conditions: The role of gel composition on their properties, Microporous Mesoporous Mater. 190 (2014) 324–333. doi:10.1016/j.micromeso.2014.02.026.

[36] G. Rioland, S. Albrecht, L. Josien, L. Vidal, T.J. Daou, The influence of the nature of organosilane surfactants and their concentration on the formation of hierarchical FAU-type zeolite nanosheets, *New J. Of Chem.*, 39 (2015) 2675-2681. doi: 10.1039/C4NJ02137A.

[37] L. Tosheva, B. Mihailova, V. Valtchev, J. Sterte, Zeolite beta spheres, Microporous Mesoporous Mater. 48 (2001) 31–37. doi:10.1016/S1387-1811(01)00327-4.

[38] K. Schumann, B. Unger, A. Brandt, F. Scheffler, Investigation on the pore structure of binderless zeolite 13× shapes, Microporous Mesoporous Mater. 154 (2012) 119–123. doi:10.1016/j.micromeso.2011.07.015.

[39] L. Itani, V. Valtchev, J. Patarin, S. Rigolet, F. Gao, G. Baudin, Centimeter-sized zeolite bodies of intergrown crystals: Preparation, characterization and study of binder evolution, Microporous Mesoporous Mater. 138 (2011) 157–166. doi:10.1016/j.micromeso.2010.09.011.

[40] S. Mintova, M. Hölzl, V. Valtchev, B. Mihailova, Y. Bouizi, T. Bein, Closely Packed Zeolite Nanocrystals Obtained via Transformation of Porous Amorphous Silica, Chem. Mater. 16 (2004) 5452–5459. doi:10.1021/cm030640b.

[41] G. Rioland, L. Bullot, T.J. Daou, A. Simon-Masseron, G. Chaplais, D. Faye, E. Fiani, J. Patarin, Elaboration of FAU-type Zeolite Beads with Good Mechanical Performances for Molecular Decontamination, RSC Advances, 6 (2016) 2470-2478. doi: 10.1039/C5RA23258A.

[42] G. Rioland, T.J. Daou, D. Faye, J. Patarin, A New Generation of MFI-type Zeolite Pellets with Very High Mechanical Performance for Space Decontamination, *Microporous and Mesoporous Materials*, 221 (2016) 167-174. doi: 10.1016/*j*.micromeso.2015.09.040.

[43] G. Rioland, H. Nouali, T.J. Daou, D. Faye, J. Patarin, Adsorption of Volatile Organic Compounds in Composite Zeolites Pellets for Space Decontamination, Adsorption, 23 (2017) 395-403. doi: 10.1007/s10450-017-9870-9.

[44] L. Tosheva, V. Valtchev, J. Sterte, Silicalite-1 containing microspheres prepared using shape-directing macro-templates, Microporous Mesoporous Mater. 35–36 (2000) 621–629. doi:10.1016/S1387-1811(99)00256-5.

[45] E.G. Fawaz, D.A. Salam, H. Nouali, I. Deroche, S. Rigolet, B. Lebeau, T.J. Daou, Synthesis of Binderless ZK-4 Zeolite Microspheres at High Temperature, Mol. J. Synth. Chem. Nat. Prod. Chem. 23 (2018). doi:10.3390/molecules23102647.

[46] T. Martin, A. Galarneau, F.D. Renzo, F. Fajula, D. Plee, Morphological Control of MCM-41 by Pseudomorphic Synthesis, Angew. Chem. Int. Ed. 41 (2002) 2590–2592. doi:10.1002/1521-3773(20020715)41:14<2590::AID-ANIE2590>3.0.CO;2-3.

[47] T. Martin, A. Galarneau, F. Di Renzo, D. Brunel, F. Fajula, S. Heinisch, G. Crétier, J.-L. Rocca, Great Improvement of Chromatographic Performance Using MCM-41 Spheres as Stationary Phase in HPLC, Chem. Mater. 16 (2004) 1725–1731. doi:10.1021/cm030443c.

[48] C. Petitto, A. Galarneau, M.-F. Driole, B. Chiche, B. Alonso, F. Di Renzo, F. Fajula, Synthesis of Discrete Micrometer-Sized Spherical Particles of MCM-48, Chem. Mater. 17 (2005) 2120–2130. doi:10.1021/cm050068j.

[49] A. Galarneau, A. Sachse, B. Said, C.-H. Pelisson, P. Boscaro, N. Brun, L. Courtheoux, N. Olivi-Tran, B. Coasne, F. Fajula, Hierarchical porous silica monoliths: A novel class of microreactors for process intensification in catalysis and adsorption, Comptes Rendus Chim. 19 (2016) 231–247. doi:10.1016/j.crci.2015.05.017.

[50] M. Mańko, J. Vittenet, J. Rodriguez, D. Cot, J. Mendret, S. Brosillon, W. Makowski, A. Galarneau, Synthesis of binderless zeolite aggregates (SOD, LTA, FAU) beads of 10, 70μm and 1mm by direct pseudomorphic transformation, Microporous Mesoporous Mater. 176 (2013) 145–154. doi:10.1016/j.micromeso.2013.04.006.

[51] Y. Ji, H. Yang, W. Yan, Strategies to Enhance the Catalytic Performance of ZSM-5 Zeolite in Hydrocarbon Cracking: A Review, Catalysts. 7 (2017) 367. doi:10.3390/catal7120367.

[52] J. Landers, G.Y. Gor, A.V. Neimark, Density functional theory methods for characterization of porous materials, Colloids Surf. Physicochem. Eng. Asp. 437 (2013) 3–32. doi:10.1016/j.colsurfa.2013.01.007.

[53] M. Thommes, K.A. Cychosz, Physical adsorption characterization of nanoporous materials: progress and challenges, Adsorption. 20 (2014) 233–250. doi:10.1007/s10450-014-9606-z.

[54] D. Massiot, F. Fayon, M. Capron, I. King, S. Le Calvé, B. Alonso, J.-L. Durand, B. Bujoli, Z. Gan, G. Hoatson, Magn. Reson. Chem. 40 (2002) 70-76. doi: 10.1002/mrc.984.

[55] M. Thommes, K. Kaneko, A.V. Neimark, J.P. Olivier, F. Rodriguez-Reinoso, J. Rouquerol, K.S.W. Sing, Physisorption of gases, with special reference to the evaluation of surface area and pore size distribution (IUPAC Technical Report), Pure Appl. Chem. 87 (2015). doi:10.1515/pac-2014-1117.

[56] J. Schick, T.J. Daou, P. Caullet, J.-L. Paillaud, J. Patarin, C. Mangold-Callarec, Surfactant-modified MFI nanosheets: a high capacity anion-exchanger, Chem Commun. 47 (2011) 902–904. doi:10.1039/C0CC03604H.

[57] I. Kabalan, G. Rioland, H. Nouali, B. Lebeau, S. Rigolet, M.-B. Fadlallah, J. Toufaily, T. Hamiyeh, T.J. Daou, Synthesis of purely silica MFI-type nanosheets for molecular decontamination, RSC Adv. 4 (2014) 37353–37358. doi:10.1039/C4RA05567E.